

Supporting Information

Concave-curvature facets benefit the oxygen electroreduction catalysis on octahedrally shaped PtNi nanocatalysts

S. Kühl^{a†}, M. Gocyla^{b†}, H. Heyen^a, S. Selve^c, M. Heggen^{b,*}, R. E. Dunin-Borkowski^b, P. Strasser^{a,*}

* Corresponding author email address: pstrasser@tu-berlin.de, m.heggen@fz-juelich.de

This Supplementary Materials includes:

- Table S1 and S3 presenting an overview on compositional data before and after electrochemistry in dependence of the annealing temperature
- Table S2 giving structural parameters of Rietveld refinement – details and parameter used for Rietveld refinement given above table
- Figure S1-S10 with additional results and information for XRD incl. Rietveld refinement, TEM particle size distributions as well as electrochemical characterization before and after stability test
- Figure S11 showing additional TEM images after electrochemistry

ICP-OES – constant PtNi composition and Pt-loading on carbon

Table S1. PtNi composition and Pt-loading in dependence of annealing temperature – comparison of ICP-OES and EDX data.

Sample	ICP-OES data			EDX data	
	Pt loading / wt%	at% Pt	at% Ni	at% Pt	at% Ni
as prepared	21	37	63	43	57
H₂ 200°C	19	37	63	38	62
H₂ 300°C	20	39	61	38	62
H₂ 400°C	20	38	62	37	63
H₂ 500°C	20	39	61	38	62

XRD evaluation

1) Details to Rietveld refinement and parameters obtained

Details to Rietveld Refinement:

- background: Chebychev with 4 polynomial coefficients
- phases:
 - Pt fcc with Pt and Ni sites as well as interstitial O
 - Pt & Ni occupancy was applied according to composition 0.4 and 0.6, respectively
 - O occupancy refined – results given in Table S2
 - additional peak phases to subtract carbon support:
 - each at 24.98° 2θ & 43.5° 2θ,
 - H₂ 400 °C additionally at 30.37° 2θ

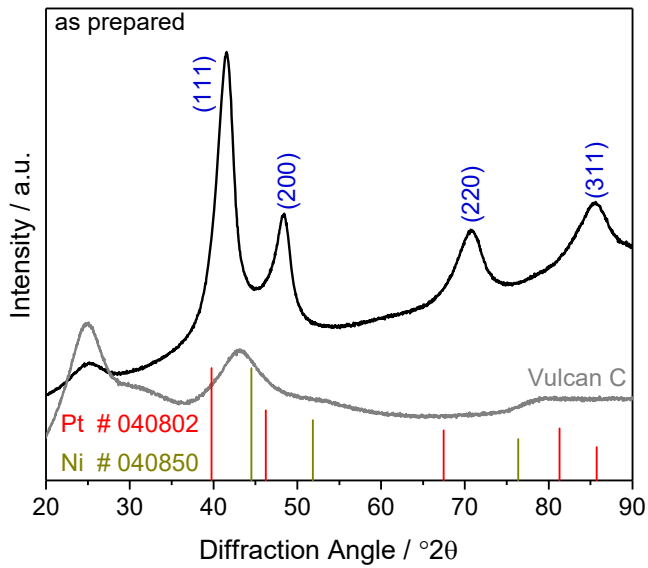


Figure S1. Influence of carbon support to PtNi alloy – shown for PtNi-prep.

Table S2. Structural parameters obtained by Rietveld refinement of XRD pattern – including the occupancy of interstitial oxygen atoms.

Sample	a / Å	strain e ₀	LVol-IB / nm	occ. (O _{int})	R _{wp}
as prepared	3.7315(45)	0.577(19)	2.966(50)	0.3133(80)	1.66
H₂ 200°C	3.7367(76)	0.686(51)	3.24(11)	0.288(15)	1.17
H₂ 300°C	3.7163(48)	0.760(37)	5.16(20)	0.2485(91)	1.33
H₂ 400°C	3.6967(81)	0.5730(36)	5.78(24)	0.246(12)	1.24
H₂ 500°C	3.692(70)	0.4680(14)	7.05(21)	0.1820(70)	1.62

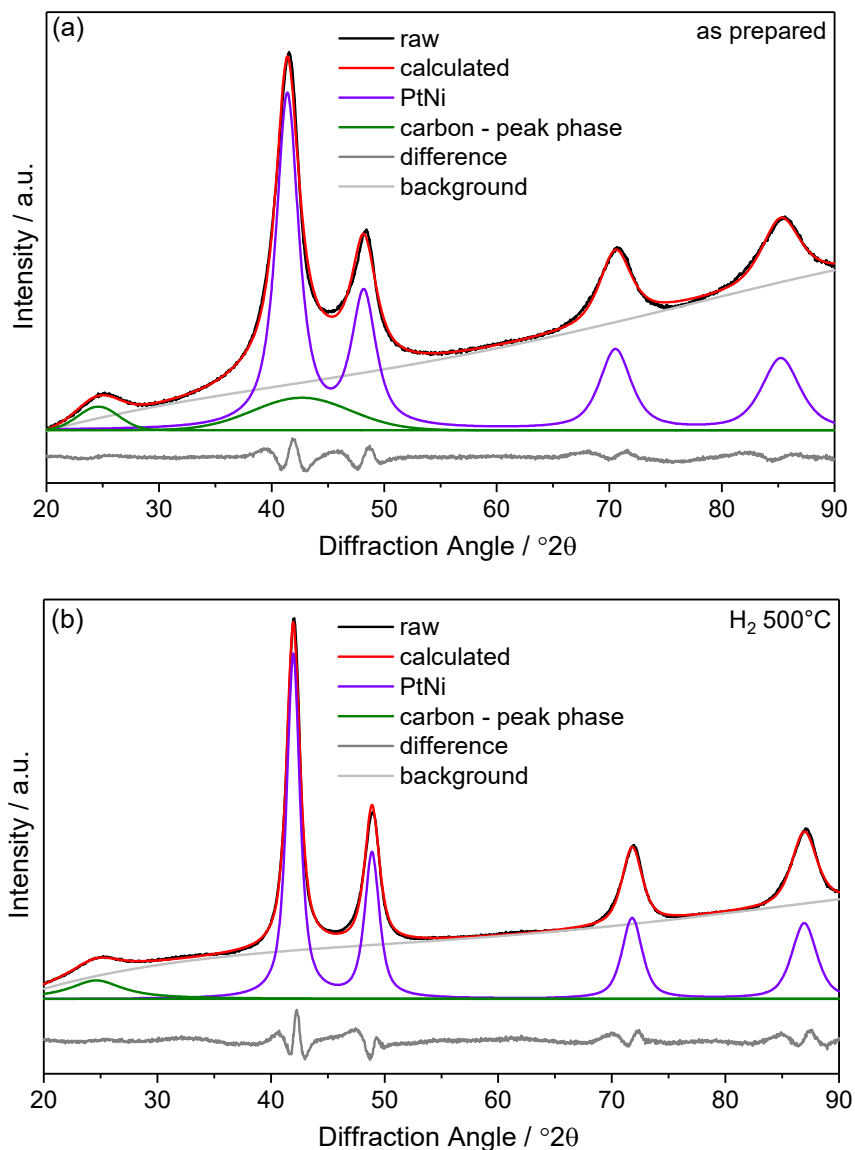


Figure S2. (a+b) Exemplary Rietveld refinement: Patterns well described with one fcc phase and carbon as peak phase - small deviations seen for as prepared sample.

2) Dependence of d value on annealing temperature

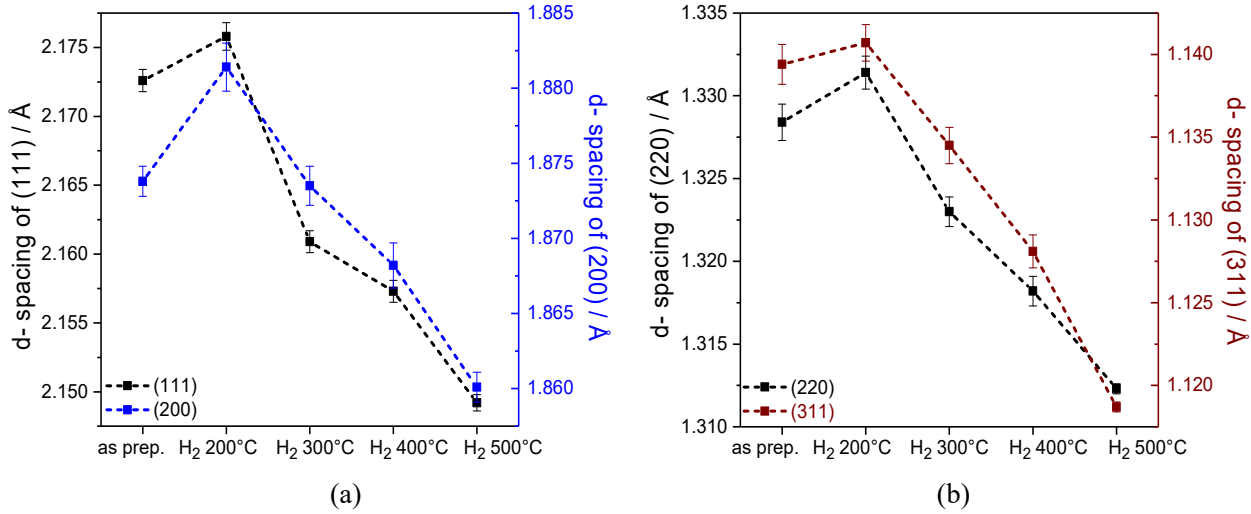


Figure S3. Change of d values in dependence of annealing temperature. Dashed lines are only a guide to the eye.

3) Additional result: strain vs. size – no clear dependence

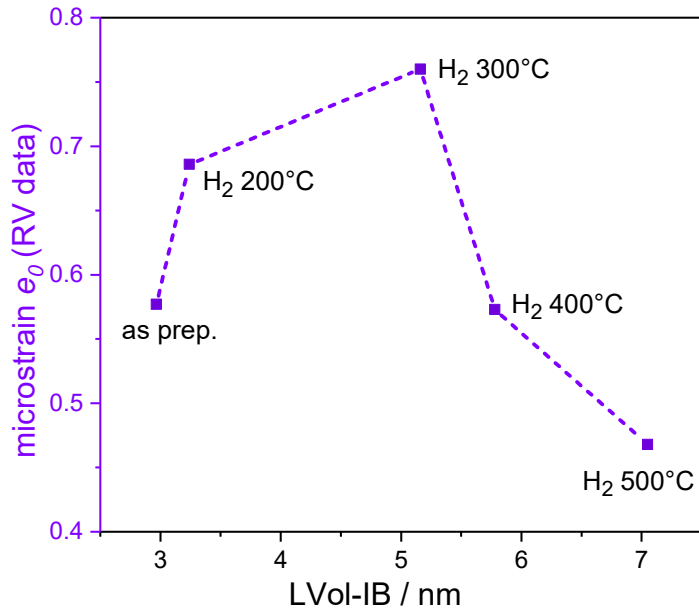


Figure S4. Result of Rietveld refinement: Strain vs. size plot – showing no clear trend of microstrain and NP size; dashed line is only a guide to the eye.

TEM particle sizes

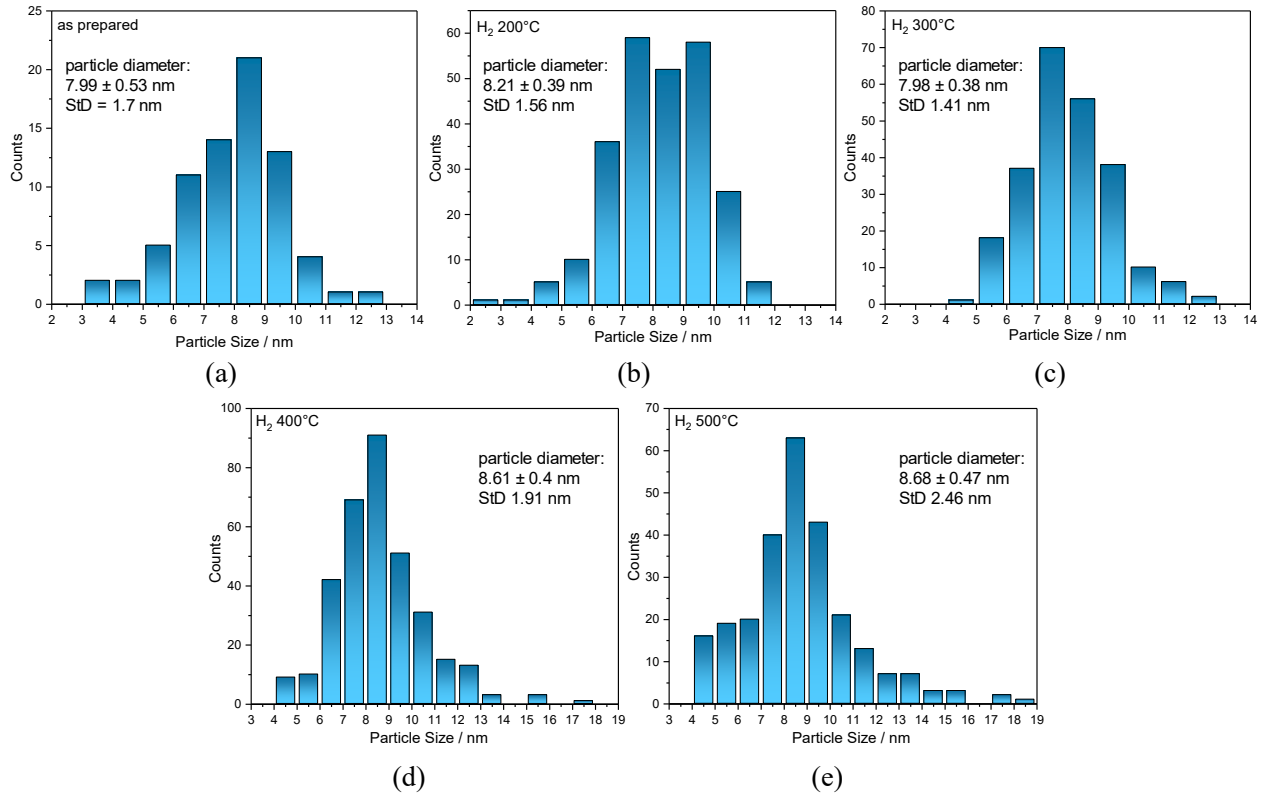


Figure S5. Particle size distributions determined from BF-TEM images – for every sample, 75-170 particles were measured. The average of the particle diameters are given with a calculated error (see explanation below), and the standard deviation (StD) of the mean is noted in addition.

The error of the particle size was determined based on an interlaboratory comparison case study,¹ adding an additional systematic error ($u(\text{sys})$):

$$u(\text{PS}) = SE + u(\text{sys}). \quad (1)$$

In the comparison case study, the standard error (SE) was derived as:

$$SE = \frac{\text{StD}}{\sqrt{n}}. \quad (2)$$

In the present study, a systematic error of the particle sizes was added to account for the uncertainty of the determination of the particle diameters, which was estimated to 0.25 nm.

Electrochemical Characterization

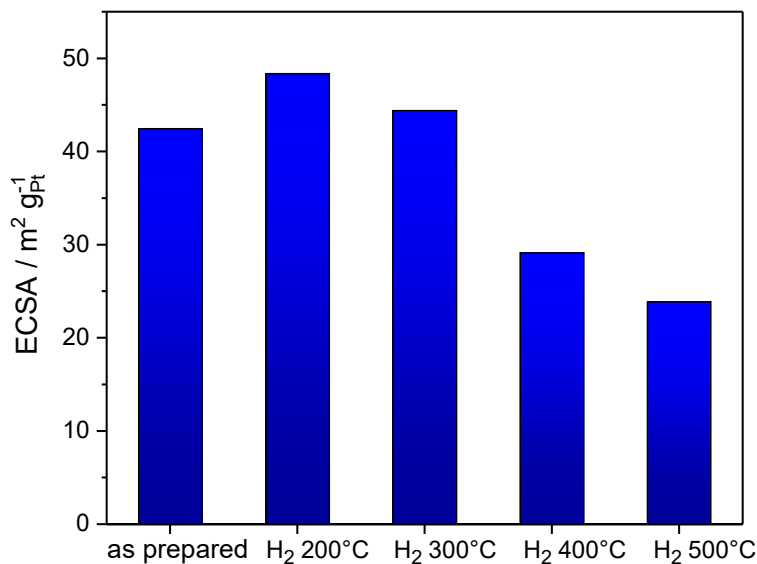


Figure S6. Electrochemical surface area in dependence of annealing temperature.

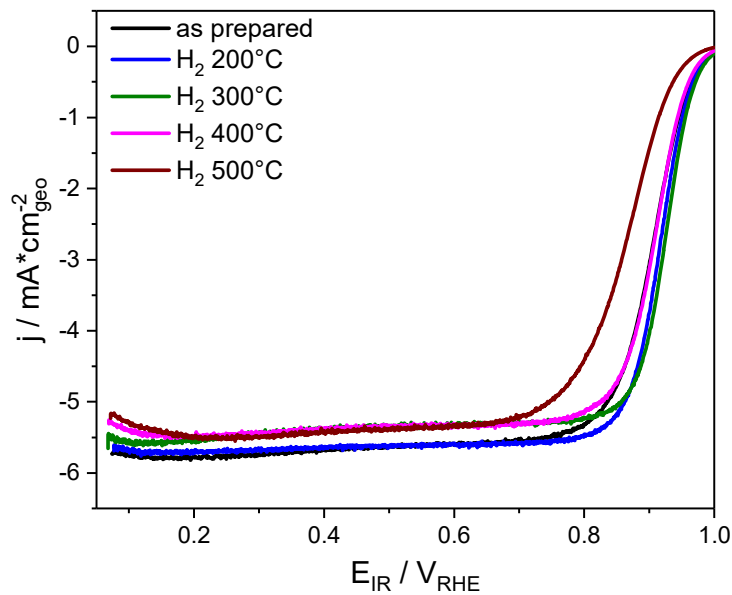


Figure S7. ORR performance in dependence of annealing temperature – linear sweep voltammograms shown. Stable performance after annealing up to 400 °C; decreased activity after 500 °C.

Additional results of stability test

1) Changes of CVs upon cyclization

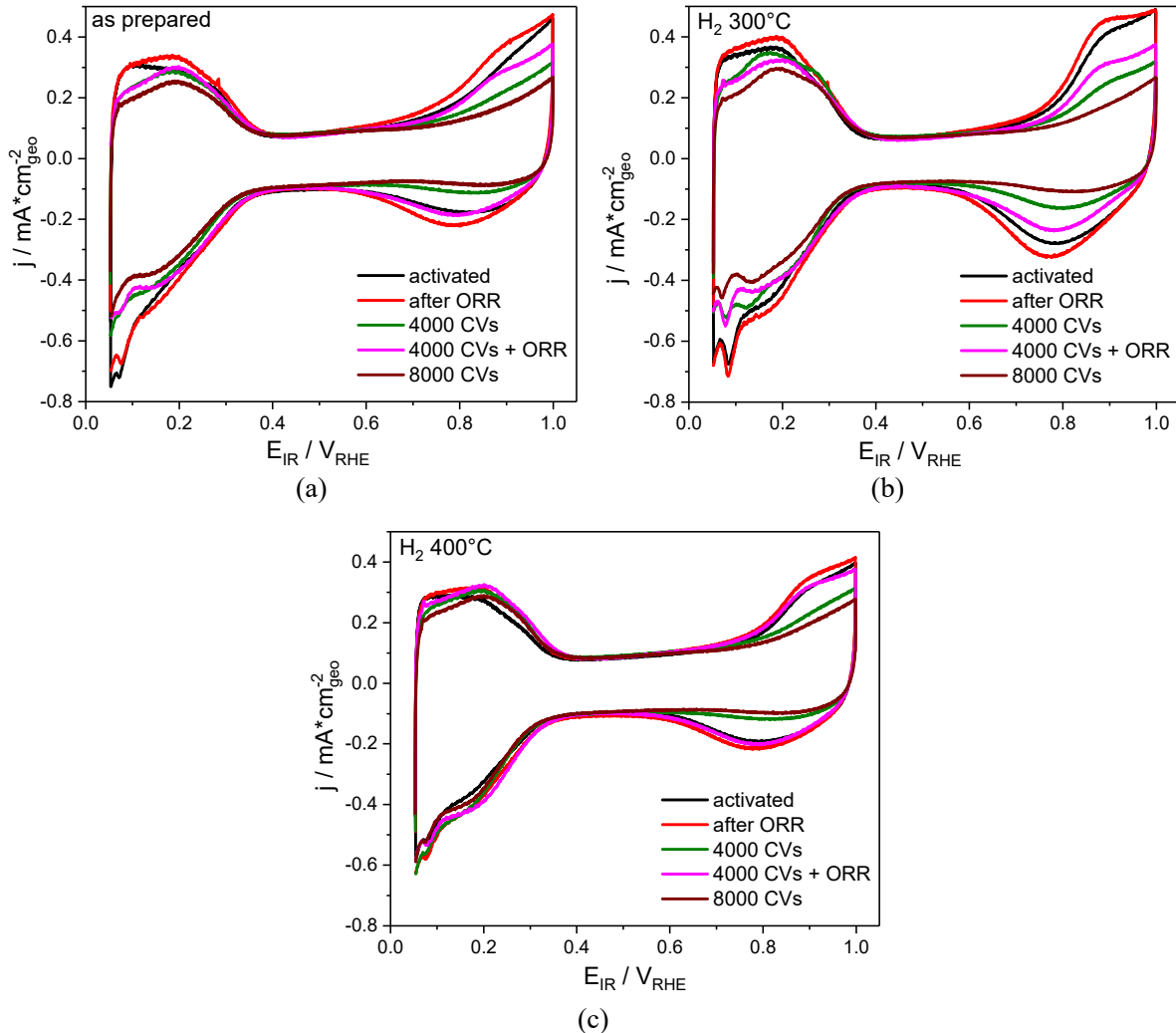


Figure S8. Changes of CVs after ORR and upon cyclization for 4000 and 8000 cycles in the potential range 0.5 – 1 V_{RHE} (50 mV s⁻¹) – exemplary shown for (a) as prepared, (b) H₂ 300°C, (c) H₂ 400°C.

2) Influence of cyclization onto LSVs

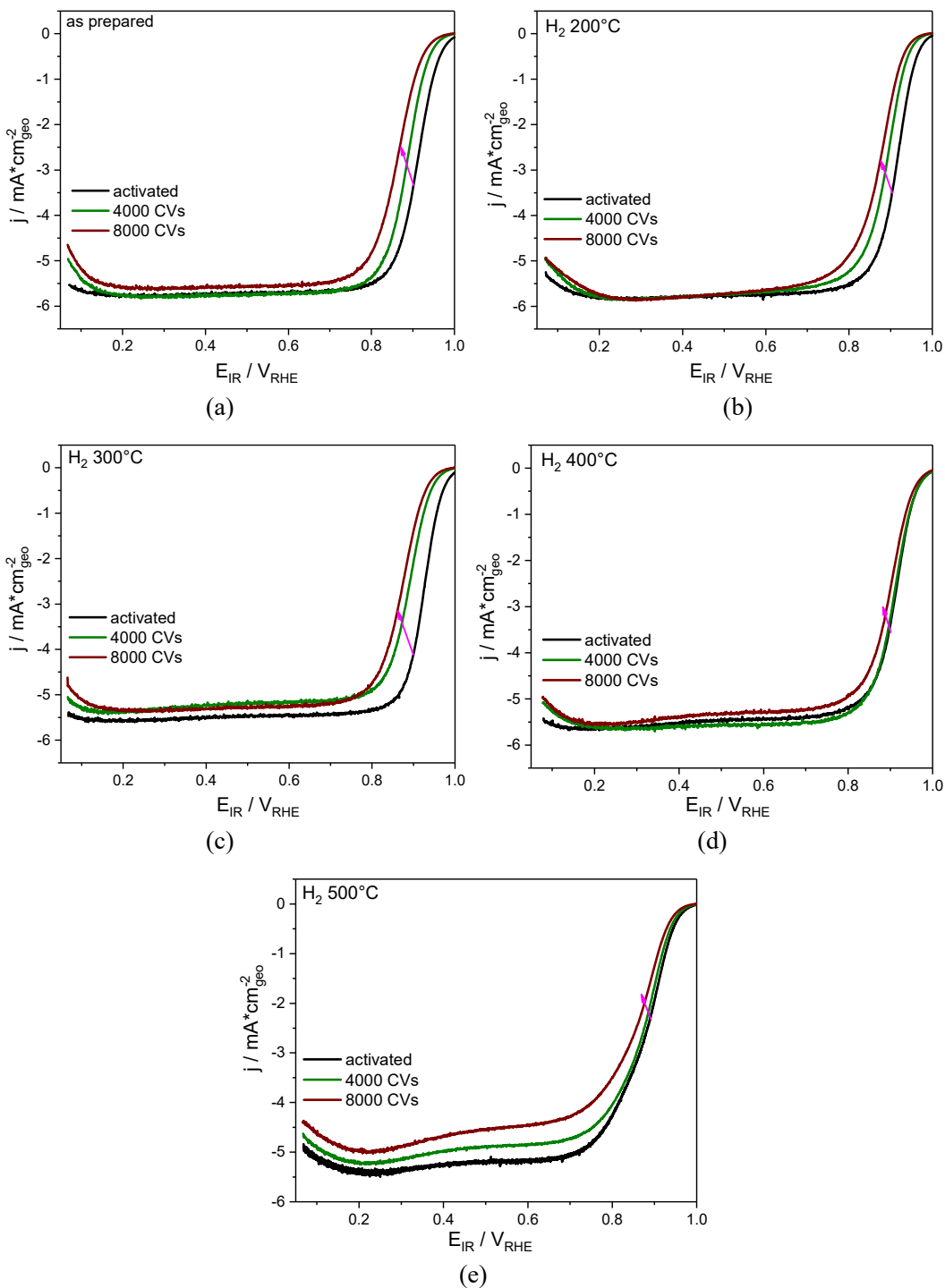


Figure S9. Stability of ORR performance upon cyclization – Linear sweep voltammograms of annealed catalysts after activation (black curves, 25 CVs) and after stability test for 4000 and 8000 cycles in the potential range 0.5 – 1 V_{RHE} (50 mV s⁻¹): a) as prepared, b) H₂ 200°C, c) H₂ 300°C, d) H₂ 400°C H₂, e) H₂ 500°C.

3) ECSA before and after cyclization

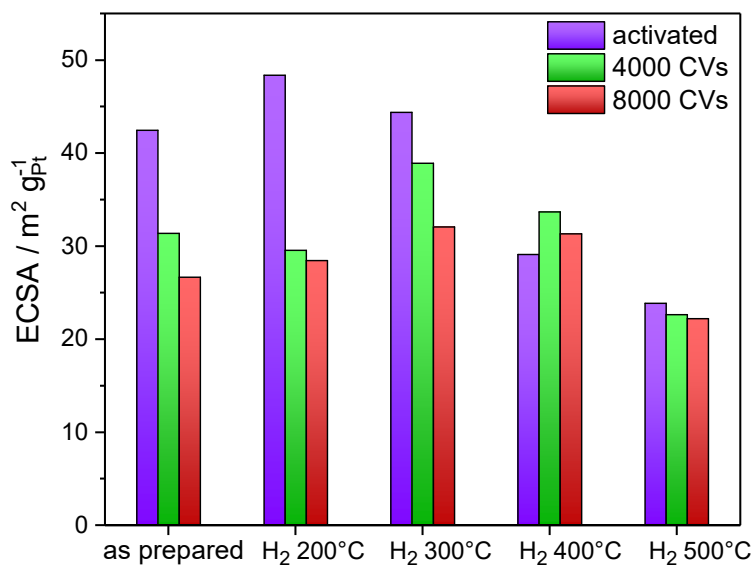


Figure S10. Stability of ECSA of annealed catalysts after stability test for 4000 and 8000 cycles in the potential range 0.5 – 1 V_{RHE} (50 mV s⁻¹).

4) Composition – before and after stability test

Table S3. PtNi composition after electrochemical cycling determined by EDX – initial data obtained by ICP-OES (see **Table S1** for comparison).

Sample	initial		after 4000 CVs		after 8000 CVs	
	at% Pt	at% Ni	at% Pt	at% Ni	at% Pt	at% Ni
as prepared	37	63	86	14	93	7
H₂ 300°C	39	61	81	19	81	19
H₂ 400°C	38	62	59	41	63	37

5) Additional TEM images after stability test

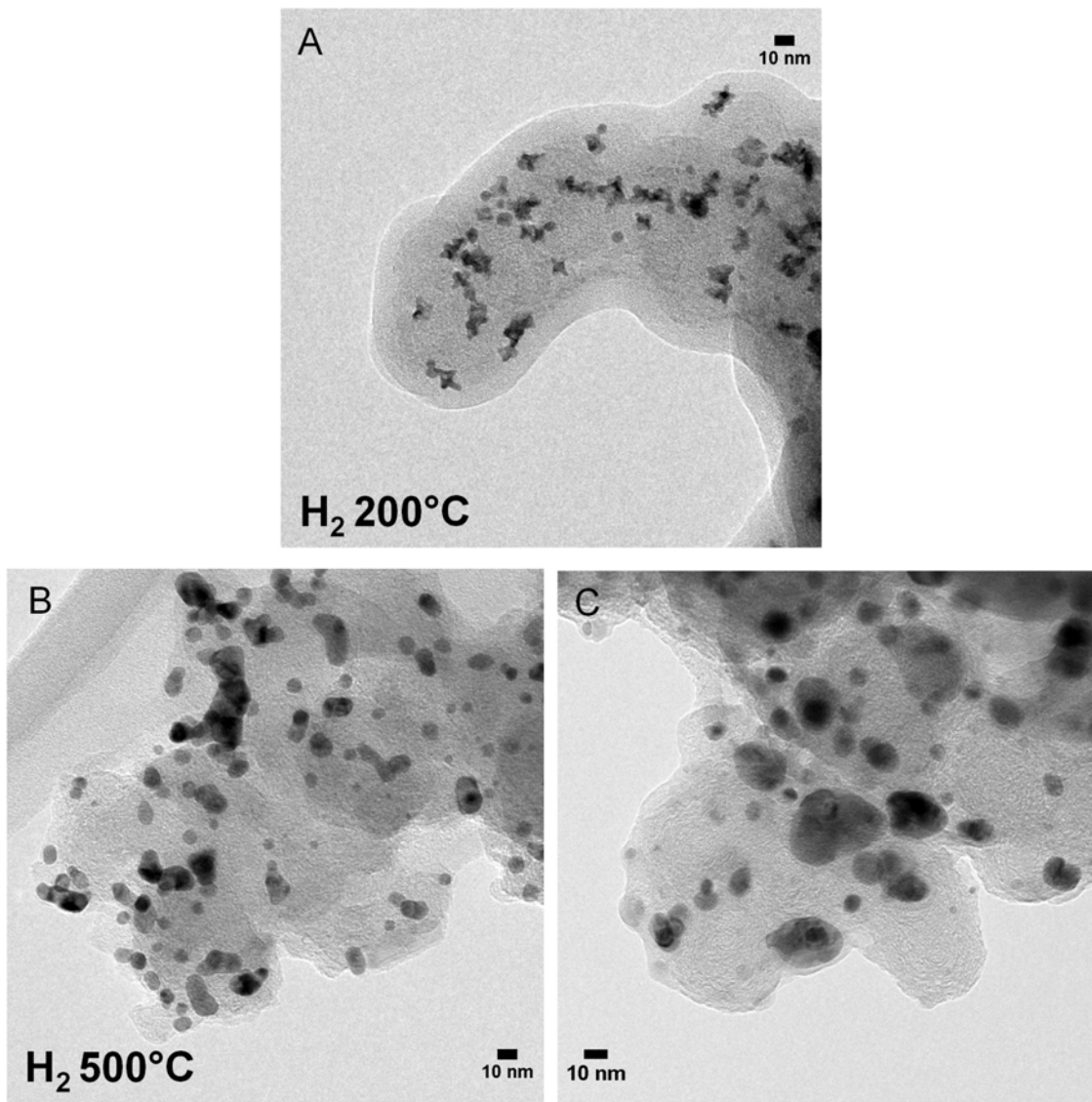


Figure S11. Change of morphology upon electrochemical treatment, images shown after 25th cycle of activation of (A) H_2 200°C and (B) H_2 500°C, and (C) H_2 500°C after 8000CVs.

References

1. S. B. Rice, C. Chan, S. C. Brown, P. Eschbach, L. Han, D. S. Ensor, A. B. Stefaniak, J. Bonevich, A. E. Vladar, A. R. H. Walker, J. W. Zheng, C. Starnes, A. Stromberg, J. Ye and E. A. Grulke, *Metrologia*, 2013, **50**, 663-678.